

17 μm molecular hydrogen line emission from OMC-1

Michael G. Burton¹ and Michael R. Haas²

¹ School of Physics, University of New South Wales, Sydney, New South Wales 2052, Australia

² Space Science Division, NASA/Ames Research Center, MS245-6, Moffett Field, California 94035-1000, USA

Received 17 March 1997 / Accepted 27 May 1997

Abstract. The $v=0-0$ S(1) line of molecular hydrogen at 17.03 μm has been measured in the source OMC-1 along a 90'' cut passing through the near-IR H₂ emission Peaks 1 and 2 using the Kuiper Airborne Observatory. The line flux is typically 50% of the 2.12 μm $v=1-0$ S(1) line, but its distribution is somewhat more extended and it is relatively brighter at Peak 2. We interpret this as shocked emission coming from two regions of roughly equal brightness and lying close to the plane of the sky, plus a more extended contribution from slower shocks ($\sim 5 \text{ km s}^{-1}$) which do not contribute significantly to the near-IR vibrational-rotational lines. The 17 μm line flux is an order of magnitude too strong to be explained by planar J- and C-shock models. However our data cannot distinguish between the merits of a cooling flow dominated by H₂ line emission and the integrated emission from a C-type bow-shock. Both models predict column density ratios close to those observed from a variety of lines covering a range from 1 000 to 25 000 K in upper state energy. We predict a flux for the ground state 28.2 μm 0-0 S(0) line of $\sim 2\%$ that of the 1-0 S(1) line at Peak 1, and suggest that a consistent set of observations of the lowest pure rotational lines of H₂ would allow us to distinguish between these shock models.

Key words: ISM: molecules – ISM: individual objects (OMC-1) – shock waves – molecular processes – techniques: spectroscopic – infrared: ISM: lines and bands

1. Introduction

The lowest lying pure-rotational lines of molecular hydrogen can be emitted from gas of much lower excitation than the near-IR lines commonly observed from molecular clouds. For instance, the 17.03 μm $v=0-0$ S(1) line, originating from an energy level 1 015 K above ground, emits strongly from gas as cool as 100 K, while a temperature greater than 1 000 K is needed for the 2.12 μm $v=1-0$ S(1) line to thermally emit. Thus the 17 μm

line is expected to be a strong coolant in warm photodissociation regions in the Galaxy, where the gas temperature is typically a few hundred Kelvin. Similarly, in shock waves as slow as $\sim 5 \text{ km s}^{-1}$, where the vibrational levels remain unpopulated, the 17 μm line can be excited, providing a probe of softer shocks which otherwise would be unobserved (Burton et al. 1992).

Mitigating against these advantages for its use in studying such environments are the poor atmospheric transmission, high thermal background and inferior detection technology compared to the near-IR. These have all served to limit observation of the mid-IR lines. Indeed, only Parmar et al. (1991, 1994) have reported detections of the 17 μm line from the ground, although the ISO satellite is now routinely detecting it (e.g., Kunze et al.; Moorwood et al.; Rigopoulou et al.; Sturm et al.; Timmermann et al.; Wright et al.; all 1997). This provides us with a new opportunity for understanding the mechanism of shock-excitation in molecular clouds.

There is considerable debate over the physical nature of shock waves (e.g., Hollenbach et al. 1989; Draine, 1991; Draine & McKee, 1993). It seems clear that bow-shocks must be common, as opposed to simple planar-shocks (e.g., Smith & Brand, 1990; Smith et al. 1991a; Smith, 1991; Burton, 1992; Brand 1995a,b), to produce a range of excitation conditions within a given region. However it is still uncertain whether these are C-type, J-type, or a combination of both. Many theoretical arguments suggest that shocks must be C-type in molecular clouds, based on the expected values of the magnetic field strengths and ionization fractions (e.g., Chernoff et al. 1982; Draine et al. 1983). Data on high-excitation lines of H₂, however, can still be fit readily by planar J-shock models where H₂ dominates the cooling (e.g., Brand et al. 1988). The low-excitation 17 μm 0-0 S(1) line, on the other hand, probes a cooler region of the shock front than do the near-IR lines. Thus it may be used to extend the range of parameter space when testing competing models.

We have used the Kuiper Airborne Observatory (KAO) to measure the 17 μm molecular hydrogen line emission from the nearby massive star forming region OMC-1. This is the brightest H₂ source in the sky, and thus has been subject to intense study. For instance, high spatial resolution mapping (Allen & Burton,

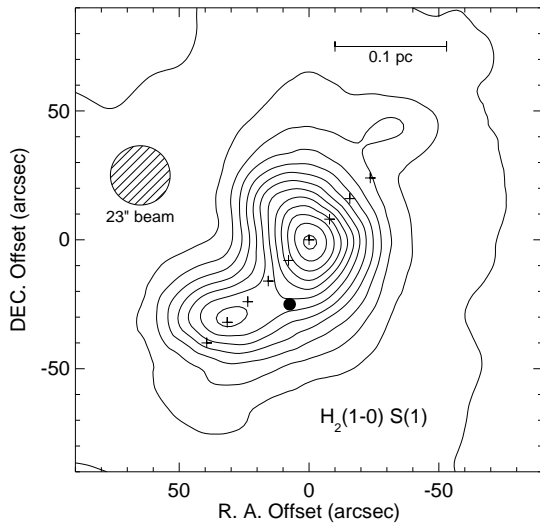


Fig. 1. The positions (+'s) observed in H₂ 0-0 S(1) are indicated on the H₂ 1-0 S(1) map of Burton & Puxley (1990). The latter has been smoothed from its original resolution of 19'' to our beam size of 23''. Offsets are from Peak 1. The position of BN/KL is marked by the ● and the scale bar represents a size of 0.1 pc at a source distance of 480 pc. The lowest contour level is $7 \times 10^{-16} \text{ W m}^{-2}$, with a step size of $3.3 \times 10^{-15} \text{ W m}^{-2}$, per 23'' beam.

1993), high-excitation line spectra (Brand et al. 1988), high-spatial resolution velocity profiles (Chrysostomou et al. 1997) and spectro-polarimetry (Chrysostomou et al. 1994) of the H₂ emission have all served to produce a picture of a complex region that is being shocked by both a steady wind and impulsive event(s) that have produced a series of compact high-velocity bow-shocks. The H₂ emission arises from two loosely bipolar lobes (Peaks 1 and 2; Beckwith et al. 1978), centred around several luminous mid-IR sources (Dougados et al. 1993). Winds and/or ejections, driven by one or more of the sources in the IRc2-complex, have resulted in the shock-excitation of ambient cloud molecular gas, producing the H₂ emission we observe. Our KAO observations of the 17 μm 0-0 S(1) line were made along a cut between the two emission lobes.

2. Observations

These data on the 0-0 S(1) line of H₂ at $17.034835 \pm 0.000006 \mu\text{m}$ (Jennings et al. 1987) were obtained with the 91 cm telescope of the KAO on the flight of February 6, 1991 using the facility cryogenic grating spectrometer (CGS; Erickson et al. 1984, 1995). The H₂ line and the adjacent continuum were simultaneously observed using an array of 26 Si:Sb impurity band conduction (IBC) detectors kindly provided by Rockwell, Inc. The aperture size was $\sim 23''$ and the spectral resolution was $\sim 55 \text{ km s}^{-1}$. Standard chopping techniques were employed throughout; sequences of right and left beams were taken with an integration time of 10 s between nods and the oscillating secondary mirror was operated in cross elevation with an amplitude of 6' and a frequency of 13 Hz.

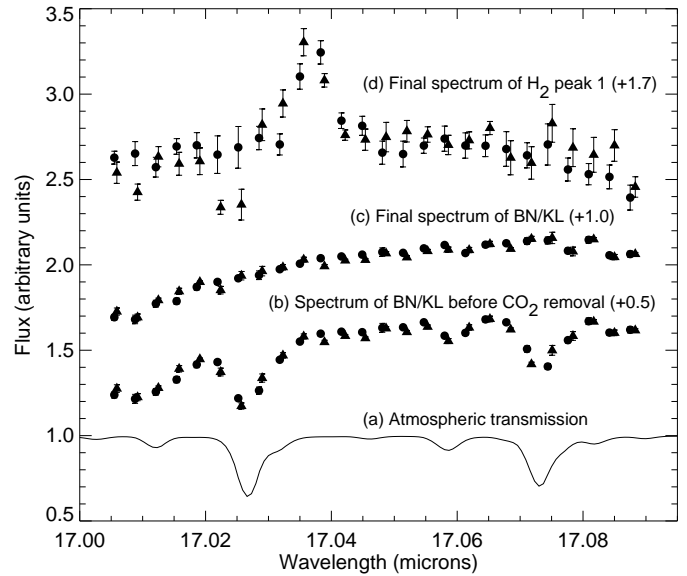


Fig. 2. Representative spectra of the H₂ 0-0 S(1) lines. They are in the rest frame of the Earth's atmosphere and have been normalized (see Table 1 for continuum levels) and then offset by the amounts indicated in parentheses: (a) model of atmospheric transmission at 41,000 ft; (b) spectrum of BN/KL before telluric correction; (c) BN/KL after correction; (d) final spectrum for Peak 1. The two symbols (triangle and circle) represent separate observations.

The observed positions include BN/KL and the 9 locations shown in Fig. 1, which lie along a line passing through H₂ 1-0 S(1) Peaks 1 and 2 with an 11'' (half beam) spacing. Two spectra were taken at each spatial location; the first centred at a wavelength of 17.0465 μm and the second at 17.0471 μm . There are six significant telluric CO₂ absorption lines within our band-pass, four of them weak (17.012, 17.031, 17.059 and 17.077 μm) and two of them strong (17.027 and 17.073 μm), with the H₂ line lying on the wing of the strongest line. Consequently, off-line (continuum) spectra were also taken on BN/KL and on Mars, which was observed for calibration. The continuum band was centred at 17.86 μm and is relatively free of telluric absorption.

The line spectra were flat fielded and fluxed by dividing by the Mars continuum spectrum and multiplying by the Mars flux, assuming a mean diameter of 9.42'' and a brightness temperature of 227.3 K (Simpson et al. 1981). The telluric lines measured against BN/KL were used to determine the best-fit wavelength scale and CO₂ overburden (the Mars on-line spectra are contaminated by CO₂ in the Martian atmosphere). The telluric CO₂ was assumed to be uniformly mixed and the plane parallel approximation was used to correct for elevation effects; the standard atmosphere was used to correct for small column-depth differences due to changes in flight altitude (41 000 to 45 000 feet). These CO₂ column densities were used to compute atmospheric models (Lord 1993), which were divided into the above ratioed spectra to remove the effects of telluric absorption. Fig. 2 shows (a) the computed atmospheric transmission at 41 000 feet for a zenith angle of 45° and a CO₂ mixing ratio of 287 ppmV; (b) the

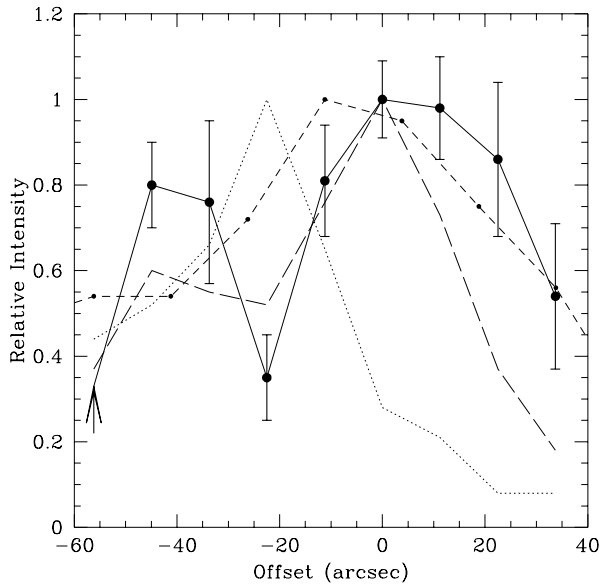


Fig. 3. Cuts of the relative intensities of the 0-0 S(1) line (large \bullet 's), 1-0 S(1) line (long dashed), 17 μm continuum (dotted) and [Si II] 35 μm line (short dashed with small \bullet 's, from Haas et al. 1991) across OMC-1. Offsets are from Peak 1.

spectrum of BN/KL before correction for telluric absorption; (c) the final, corrected spectrum of BN/KL; and (d) the final, corrected spectrum of H₂ Peak 1. The difference in instrumental response between the line and continuum wavelengths has been removed using ratios of laboratory spectra at the same grating positions and verified by the flat baselines obtained for BN/KL (Fig 2c) and Mars. A small diffraction correction has been applied to account for differences in source size.

The H₂ 1-0 S(1) line is not detected at BN/KL because of the strong continuum. A small misalignment in the instrument gives the detectors slightly different fields of view, often resulting in curved baselines such as those shown in Fig. 2. These were removed during the line fitting procedure by dividing out a low-order polynomial fit from the continuum data. The continuum intensities were determined by averaging the detector channels containing no line emission. The line intensities were obtained by summing the channels containing line emission, multiplying by the width of a detector, and subtracting the average continuum level. The final results are listed in Table 1. The quoted errors are statistical only and represent one standard deviation of the mean. They do not include the absolute calibration error, which is estimated to be $\pm 30\%$ (3σ).

3. Results

Typical line intensities measured for the 0-0 S(1) line are of order $1-2 \times 10^{-14} \text{ W m}^{-2}$ per $23''$ beam, about half the intensity of the 1-0 S(1) line through the same aperture. The lines are resolved, their average FWHM being $\sim 108 \text{ km s}^{-1}$, subtracting the instrumental resolution from the measured FWHM of $\sim 121 \text{ km s}^{-1}$. The measured line widths and Doppler shifts are

consistent with those measured for the 1-0 S(1) line. However our S/N is insufficient to examine whether there is a gradient in peak velocity between Peak's 1 & 2, as measured for the 1-0 S(1) line ($+8$ to $+13 \text{ km s}^{-1}$; Chrysostomou et al. 1997).

Fig. 3 presents the relative intensity of the 0-0 and 1-0 S(1) lines along a cut through Peak 1 and 2, together with that of the 17 μm continuum. The 35 μm [Si II] line, taken with a similar cut and aperture by Haas et al. (1991), is also shown. The 17 μm line distribution clearly follows that of the 2 μm line, with the strong mid-IR continuum peaking between the two lobes. In detail, there is some suggestion that the 17 μm line is both more extended than the 2 μm line and relatively stronger towards Peak 2. The H₂ line distribution is broadly consistent with that of the [Si II] 35 μm line, although the latter line shows a single wide peak across OMC-1 and not the secondary Peak 2.

The 0-0/1-0 S(1) line ratio of 0.45 ± 0.05 at Peak 1 in the $23''$ KAO beam is slightly larger than that determined in smaller beam measurements, 0.39 ± 0.07 (from a 0-0 S(1) line intensity of $3.3 \pm 0.6 \times 10^{-3} \text{ ergs s}^{-1} \text{ cm}^{-2} \text{ sr}^{-1}$ in a $4''$ aperture (Parmar et al. 1994) and a 1-0 S(1) intensity of $8.5 \times 10^{-3} \text{ ergs s}^{-1} \text{ cm}^{-2} \text{ sr}^{-1}$ in a $5''$ aperture (Brand et al. 1988)). This also indicates the extended nature of the 17 μm line emission. The relative intensity we measure for the 0-0 S(1) emission between Peaks 1 and 2 is 1.3 ± 0.3 , slightly larger than the ratio of $1.0_{-0.3}^{+0.4}$ measured by Parmar et al. (1994). However this likely reflects the more compact size of the Peak 2 emission region seen in two very different sized apertures.

Furthermore the 0-0 S(1) line strength in OMC-1 is found to be typically an order of magnitude brighter than in other bright Galactic sources, such as S140 (Timmermann et al. 1997) and Cepheus A (Wright et al. 1997). OMC-1 is by far the easiest H₂ line emission source to study at mid-IR wavelengths, as in the near-IR.

4. Discussion

The broad lines and similar distribution to the 2 μm line clearly indicates that the bulk of the 0-0 S(1) line emission has been shock-excited, originating from the same regions as the 1-0 S(1) line. Its slightly more extended distribution may result from a contribution by 'soft-shocks', those with speeds of $\sim 5 \text{ km s}^{-1}$. Such shocks are too slow to excite any vibrational-rotational levels, but sufficient to populate the first few rotational levels of the ground vibrational state (Burton et al. 1992).

The 17 μm flux distribution is also similar to that of the 35 μm [Si II] line, providing further evidence that it has been shock-excited. Haas et al. (1991) argue that the [Si II] flux is enhanced in OMC-1 due to shock-excited emission overlaying a broader component from the photodissociation region (PDR) surrounding the M42-Trapezium III region. The [Si II] line does not, however, show the double peak morphology of the H₂ lines. Haas et al. argue that this results from a combination of faster shocks closer to the central source(s) and a decreasing gas-phase silicon abundance moving away from them. This is consistent with our deduction that it is the increasing contribution of slower shocks further from the sources that causes

Table 1. Line intensities in OMC-1

RA Offset ¹ arcsec	Dec Offset ¹ arcsec	0-0 S(1) Flux ² /10 ⁻¹⁴ Wm ⁻²	1-0 S(1) Flux ³ /10 ⁻¹⁴ Wm ⁻²	Continuum ⁴ Jy
39.4	-40.0	< 0.6 \pm 0.2 ⁵	1.6	7 800 \pm 60
31.5 ⁶	-32.0	1.5 \pm 0.2	2.4	9 300 \pm 60
23.6	-24.0	1.4 \pm 0.3	2.3	11 900 \pm 100
15.7	-16.0	0.6 \pm 0.2	2.2	17 900 \pm 90
7.9	-8.0	1.5 \pm 0.2	3.2	11 600 \pm 90
0.0 ⁷	0.0	1.8 \pm 0.2	4.1	5 000 \pm 40
-7.9	8.0	1.8 \pm 0.2	3.0	3 700 \pm 80
-15.7	16.0	1.6 \pm 0.3	1.5	1 400 \pm 70
-23.6	24.0	1.0 \pm 0.3	0.8	1 400 \pm 90
7.5 ⁸	-25	< 0.8 \pm 0.3 ⁵	1.9	42 800 \pm 200

1. Offsets in arcseconds from Peak 1 at 05^h32^m46.2^s, -05°24'02" (1950).
2. Through the 23" beam of the KAO.
3. Through a 23" beam, smoothed from the 19" beam of Burton & Puxley (1990).
4. Adjacent continuum at 17 μm , through 23" beam (this work).
5. 3 σ upper limit.
6. Peak 2.
7. Peak 1.
8. BN/KL.

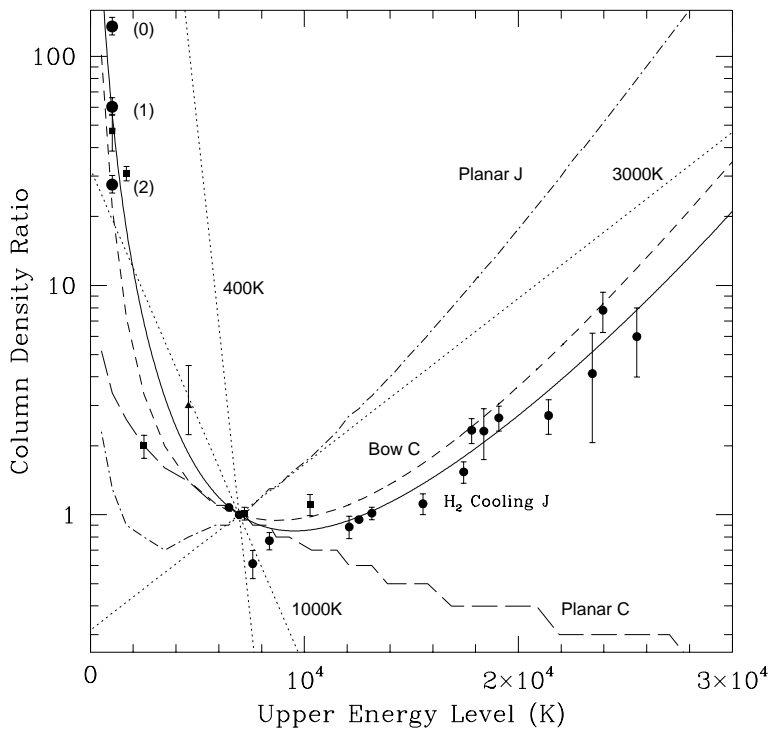


Fig. 4. Column density ratios (*CDR*, as defined in the text) for H₂ to Peak 1 plotted against upper energy level. The large ●'s are our measurements for the 0-0 S(1) line for 0, 1 and 2 magnitudes of extinction at 2.12 μm , as labelled. The small ●'s are from Brand et al. (1988), the squares are from Parmar et al. (1994) and the triangle is from Beckwith et al. (1983), all assuming 1 magnitude of extinction at 2.12 μm . Overlaid are the planar J-shock model with H₂ cooling (solid line; Brand et al. (1988), Burton et al. (1989)) and the models of Smith (1991) for planar C-shocks (long dashes), planar J-shocks with conventional cooling (dot-dashes), and a C-type bow-shock (short dashes). In addition, the straight dotted lines show the *CDR* for gas in LTE at a single temperature (labelled 400, 1000 and 3000 K, respectively), with 2000 K gas having *CDR* = 1.

the more extended distribution at 17 μm than 2 μm . Silicon can be expected to be most depleted from the gas-phase where the grains have experienced minimal destruction, which would be where the shocks are weakest.

The higher ratio of 0-0/1-0 S(1) line flux from Peak 2 than Peak 1 might arise due to extra extinction to Peak 2. If the intrinsic line ratios from these two Peaks are the same, then this

corresponds to an additional extinction of 0.35 ± 0.30 magnitudes at 2.12 μm towards Peak 2. This estimate has a large uncertainty, but is consistent with Peak 1 and 2 having similar intrinsic 1-0 S(1) line flux. If so, it would require that the extra differential extinction at 2.12 μm to Peak 2 be 0.55 magnitudes. Furthermore, Brand et al. (1988) have estimated that the total extinction to Peak 1 at 2.12 μm is ~ 1 magnitude. These estimates

Table 2. Values of the ‘Column Density Ratio’ *CDR* for the 0-0 S(1) line for a range of assumed extinctions

Extinction ¹ (magnitudes)	<i>CDR</i> ²
0.0	135 \pm 12
0.5	91 \pm 8
1.0	61 \pm 6
1.5	41 \pm 4
2.0	27 \pm 3

1. Extinction at 2.12 μm .

2. *CDR* is determined by Eq. 2.

then imply that the column of gas to Peak 2 is $\sim 50\%$ greater than Peak 1. Chrysostomou et al. (1997) have argued, based on H₂ radial velocity measurements, that the Peak 2-Peak 1 axis is only inclined a few degrees from the plane of the sky. The average gas density in the emitting regions would then have to be of order 10⁵ cm⁻³ to provide the necessary columns of obscuring material. This density is typical of that estimated for the high-velocity molecular outflow (see Genzel & Stutzki, 1989).

4.1. Column Density Ratios (*CDR*)

It is of interest to compare the measurements of the 0-0 S(1) flux at Peak 1 to the predictions of various shock models for the source. To do so, we calculate the ‘column density ratio’ (*CDR*) for a level *j*, which is the model’s prediction for the ratio of the column density, N_j , to that of the (*v*,*J*)=(1,3) level, N_1 , (producing the 1-0 S(1) line), and divided by the same quantity for gas in LTE at 2 000 K; i.e.,

$$CDR = \left(\frac{N_j/N_1}{(N_j/N_1)_{2000}} \right) = \left(\frac{N_j g_1}{N_1 g_j} \right) e^{\left(\frac{T_j - T_1}{2000} \right)}. \quad (1)$$

This can be directly related to the data by substituting the observed line intensity, I_j for the column density:

$$CDR = \left(\frac{I_j \lambda_j A_1 g_1}{I_1 \lambda_1 A_j g_j} \right) e^{\left(\frac{T_j - T_1}{2000} \right)} e^{-\Delta\tau}. \quad (2)$$

Here λ is the wavelength, A the level decay rate, g the degeneracy (including the ortho to para ratio, taken to be 3), T the upper energy level (in K) and $\Delta\tau$ the differential extinction between the emitting wavelengths. We compare the results of the model with measured values of *CDR* for a range of energy levels. For instance, if the gas was in LTE at 2 000 K, we would obtain a horizontal line with y-axis value unity. Plotted logarithmically, gas in LTE at other temperatures is represented by a straight line whose gradient increases as the temperature increases (see Fig. 4).

In Fig. 4 we plot our determination of *CDR* for the 0-0 S(1) line at Peak 1, together with values determined from

the data of Beckwith et al. (1983), Brand et al. (1988) and Parmar et al. (1994),¹ with energy levels from 1 000 to 25 000 K above ground. The excess emission for high-excitation lines can clearly be seen, indicating substantial amounts of gas present hotter than 2 000 K (the ‘canonical’ temperature for the source, as first determined by Beckwith et al. (1978) from the ratio of $v=1$ and 2 lines). This result lead Brand et al. to propose their cooling flow model for the emission. However it is now also clear that there is excess emission from the 0-0 S(1) line, indicating that substantial quantities of gas are emitting at temperatures much less than 2 000 K as well.

The *CDR* diagram makes it apparent that calculating an excitation temperature between two levels has limited applicability towards defining the physical state of the gas. The molecular hydrogen passes through a wide range of temperatures, from a few hundred to several thousand Kelvin, as it is heated and cools during passage of the shock. For instance, by examining the slope of the *CDR* curve, it is seen that the rotational excitation temperature determined from the first few levels of $v=0$ will be quite different (much less than) the vibrational excitation temperature between $v=1$ and 2.

The extinction to Peak 1 has been estimated as 1 magnitude at 2.12 μm , but is uncertain and so we plot *CDR* for the 17 μm line for a range of extinctions from 0-2 magnitudes at 2.12 μm . Our measured value of *CDR* for the 17 μm line thus varies from 135 to 27 for this extinction range (see Table 2), with a best estimate of 61 \pm 6 for 1 magnitude of extinction at 2.12 μm .

4.2. Comparison to shock models

Also shown in Fig. 4 are the predictions of four different classes of shock model. The first is a 1D planar J-shock, with cooling dominated by H₂ lines, where the only free parameter is the driving pressure behind the shock (Brand et al. 1988; Burton et al. 1989)². In it *CDR* has the value 57 for the 0-0 S(1) line. This model should be regarded as empirical. It provides an excellent fit to the near-IR data, and represents the behaviour of a partially dissociating J-shock. We will refer to it as the ‘H₂ cooling flow’ model. However, theoretical expectations are that such shocks do not exist (e.g., see Hollenbach et al. (1989)). It is provided to illustrate the contrast with three other classes of models, for which representative predictions from the models of Smith (Smith 1991; Smith et al. 1991a, 1991b) are shown. These are a planar J-shock with cooling controlled by trace species rather than H₂, a planar C-shock and a C-type bow-shock. From Fig. 4, it is quite clear that the two planar shocks here cannot provide a

¹ We have assumed an extinction of 1 magnitude to the 1-0 S(1) line at 2.12 μm , as measured by Brand et al. (1988), together with an extinction law varying as $\lambda^{-1.75}$ from 2-7 μm , and a mid-IR extinction curve for astronomical silicates between 7-28 μm , as specified by Draine (1989), with $A(9.7 \mu\text{m}) = 0.54 \times A(2.12 \mu\text{m})$.

² The H₂ cooling J-shock model shown in Fig. 4 used a driving pressure $n_0 T = 8 \times 10^{10} \text{ cm}^{-3} \text{ K}$. However, while the intensities of high v -J H₂ lines are somewhat sensitive to the value of this parameter, the low-level lines are insensitive to it.

Table 3. Variation in *CDR* for 0-0 S(1) line with CO/H₂ abundance

CO/H ₂ Abundance	<i>CDR</i>
0	422
1×10^{-6}	261
1×10^{-5}	97
3×10^{-5}	51
1×10^{-4}	22 ¹
1×10^{-3}	7 ¹

1. Fit is not satisfactory for high-(v,J) H₂ lines.

satisfactory match to the data, while the integrated C-bow shock model does.

4.2.1. Cooling flows

The essential difference between C- and J-shocks, for the purposes of this discussion, is that a C-shock behaves much more closely like a single temperature slab of gas than does a J-shock. The latter is a ‘cooling flow’, the temperature of the H₂ cooling from its post-shock value of ~ 4000 K (above which it rapidly dissociates). Furthermore, for such a cooling flow significantly greater columns of warm molecular hydrogen, radiating mid-IR line emission, are produced when cooling by trace species (such as H₂O and O), is suppressed. Hence the difference between the conventional planar J-shock and the H₂ cooling flow. This is illustrated in Fig. 4 by the much larger value of *CDR* for the lowest excitation levels in the H₂ cooling flow. While uncertainties remain in the determination of *CDR* for the 0-0 S(1) line, it is clear that the 17 μm line flux is consistent with that expected from our empirical fit of a simple H₂ cooling, planar J-shock.

4.2.2. Bow shocks

Alternatively, bow shock models can also replicate the observed cooling curve. In these the total H₂ line emission is integrated along the length of a bow, with the shock speed varying from fast enough to completely dissociate the molecules at its head, to slow enough to just excite it in its tail. By choice of a suitable bow shape, or by adjustment of the abundance of trace species contributing to the cooling, the observed *CDR*-curve can be reproduced.³ Bow models have been able to replicate the very broad (~ 150 km s⁻¹ FWZI) H₂ line profiles seen in OMC-1 (Smith, 1991), much greater than the planar-shock dissociation speed, but only by requiring extremely high values of the magnetic fields, some tens of milligauss. Such field strengths raise the problem of how the gas remains confined, since the magnetic

³ The model presented here, from Smith (1991), has a parabolic bow, moving at 100 km s⁻¹ into a medium with a density of 2×10^6 cm⁻³, an Alfvén speed of 20 km s⁻¹, an ionization fraction of 2×10^{-7} and abundances for O, CO and C of 5×10^{-5} , 5×10^{-5} and 10^{-4} that of hydrogen. Choosing higher values for the abundances produces relatively more intense high-excitation H₂ line emission than this model.

pressure will then be much greater than the turbulent and thermal pressure in the pre-shock gas. Furthermore, *CDR* plots for observations which spatially resolve bows seen in the ‘fingers’ of OMC-1 (Allen & Burton, 1993) would then be expected to show significant excitation changes along them. This does not appear to occur (Tedds, 1996).

4.2.3. Cooling function for low temperatures

It should be noted that the specific prediction of the H₂ cooling flow discussed above also depends on the CO/H₂ abundance ratio. This alters the fraction of the cooling which occurs from CO lines and the lowest rotational H₂ lines when the temperature is below 1000 K. The models presented above assumed an abundance ratio for CO/H₂ of 2.5×10^{-5} . However varying the ratio from 0 to 10^{-3} causes the predictions for *CDR* to change from 422 to 7 (see Table 3) (although it should be noted that the higher abundances do not provide a satisfactory fit to the data), greater than the range when altering the extinction from 0 to 2 magnitudes. While this exercise should not be used to infer the CO abundance, it is indicative of the importance of determining the right contribution to the cooling from the trace species before it is possible to distinguish between shock models. In principle, with accurate measurements of all the pure rotational lines, including the 0-0 S(0) line, together with a reliable extinction estimate and a more complete treatment of the cooling for $T \leq 100$ K (including, in particular, that from H₂O), this method could be turned around to yield the CO/H₂ abundance ratio.

4.3. Predictions for pure rotational lines

We make use of the *CDR* diagram to predict the intensities of the pure rotational lines of H₂ in OMC-1, several of which have not yet been observed, including the fundamental 0-0 S(0) line. This line arises from only 510 K above ground and would prove to be even more effective than the 0-0 S(1) line for studying warm molecular gas if it could be routinely observed. In Table 4 we list the *CDRs* determined from our empirical H₂ cooling flow model, and from the C-bow model of Smith (1991) described earlier. From these we can estimate the intensity of a line relative to the 1-0 S(1) line for measurements through the same aperture, applying a differential extinction to the emitting wavelengths as described in Sect. 4.1. We predict the 0-0 S(0) line to be $\sim 2\%$ of the strength of the 1-0 S(1) line at Peak 1, based on the H₂ cooling flow model.

Table 4 also lists the intensities relative to the 1-0 S(1) line of all pure rotational lines that have been observed in OMC-1. The most recent measurements have been used in cases where there were multiple observations of one line by different groups. These observations, through a variety of apertures, were all scaled to a 5'' aperture (through which most measurements were made), based on multi-aperture measurements of the 1-0 S(1) line. The scaling factors so determined are listed in the table. All the lines are also shown in the *CDR* plot of Fig. 4. Only one point, for the 0-0 S(3) line, lies significantly off the H₂ cooling

Table 4. Predictions for pure rotational H₂ line fluxes in OMC-1 Peak 1

Line	Wavelength (μm)	T _{upper} (Kelvin)	Predicted ¹ <i>CDR</i> H ₂ Cooling Flow	Predicted ¹ <i>CDR</i> C-Bow Shock	Predicted ² Relative Intensity	Measured ³ Relative Intensity
1-0 S(1)	2.122	6952	1.0	1.0	1.0	1.0 ⁴
2-1 S(1)	2.248	12551	0.98	1.2	8.8(-2)	8.6 \pm 0.3(-2) ⁴
0-0 S(0)	28.22	510	241	102	2.1(-2)	
0-0 S(1)	17.04	1015	57	22	4.2(-1) 3.5 \pm 0.7(-1) ⁶	4.5 \pm 0.4(-1) ⁵ ,
0-0 S(2)	12.28	1682	18	7.3	2.9(-1)	2.9 \pm 0.2(-1) ⁶
0-0 S(3)	9.665	2504	6.9	3.4	9.5(-1)	2.7 \pm 0.3(-1) ⁶
0-0 S(4)	8.026	3476	3.3	2.0	5.4(-1)	
0-0 S(5)	6.909	4587	1.8	1.4	1.5	2.4 \pm 0.8 ⁷
0-0 S(6)	6.109	5833	1.2	1.1	4.4(-1)	
0-0 S(7)	5.511	7199	0.97	0.99	1.1	1.1 \pm 0.1 ⁶
0-0 S(8)	5.053	8682	0.86	0.94	2.9(-1)	
0-0 S(9)	4.695	10262	0.86	0.98	6.9(-1)	8.9 \pm 1.0(-1) ⁶
0-0 S(10)	4.410	11940	0.94	1.1	1.7(-1)	
0-0 S(11)	4.181	13703	1.1	1.3	3.9(-1)	
0-0 S(12)	3.995	15541	1.4	1.7	9.3(-2)	7.6 \pm 0.9(-2) ⁴
0-0 S(13)	3.846	17444	1.8	2.3	2.0(-1)	1.7 \pm 0.2(-1) ⁴
0-0 S(14)	3.724	19405	2.5	3.2	4.5(-2)	
0-0 S(15)	3.625	21413	3.5	4.8	9.0(-2)	7.0 \pm 1.3(-2) ⁴
0-0 S(16)	3.548	23460	5.2	7.5	2.0(-2)	1.6 \pm 0.8(-2) ⁴
0-0 S(17)	3.486	25540	7.8	12	3.9(-2)	3.0 \pm 1.0(-2) ⁴
0-0 S(18)	3.438	27645	12	20	8.5(-3)	

1. See Eq. 1.

2. Intensity relative to 1-0 S(1) line for observations through the same aperture, with $A_{2.12} = 1$ mag, and extinction laws as described in the text. This has been derived from the best fit H₂ cooling flow model, whose *CDRs* are given in column 4. A CO/H₂ abundance of 2.5×10^{-5} and driving pressure of $n_0 T = 8 \times 10^{10} \text{ cm}^{-3} \text{ K}$ were used.

3. Measured intensity relative to the 1-0 S(1) line. Specific intensities have been scaled to the aperture used by Brand et al. (1988), as specified below. The scaling factors were derived from a variety of 1-0 S(1) line measurements to Peak 1 through different apertures.

4. Brand et al. (1988); 5'' square aperture, scaling factor 1.0.

5. This work; 23'' circular aperture, scaling factor 2.1.

6. Parmar et al. (1994); 4'' and 2'' square apertures, scaling factor 0.9.

7. Beckwith et al. (1983); 26'' circular aperture, scaling factor 2.3.

flow curve. Its emitting wavelength, however, is at the peak of the mid-IR extinction and suffers from strong telluric contamination by ozone.

While the available data do not allow us to discriminate between our empirical H₂ cooling flow model and a bow C-shock, it is clear that a consistent set of data for all of the pure rotational lines taken with a single instrument could do so. For the lines up to 0-0 S(4) there is over a factor of two difference between the predictions of these two models. It is hoped that the ISO satellite may prove up to this challenge.

5. Conclusions

We have observed the 17.03 μm 0-0 S(1) line of molecular hydrogen along a cut running between the two bright H₂ emission peaks, Peaks 1 and 2, of the source OMC-1. We have come to the following conclusions from this study:

1. The 0-0 S(1) line is typically 50% as strong as the 2.12 μm 1-0 S(1) line. Our measurements are consistent with the earlier work of Parmar et al. (1994) who observed the line with much higher spatial resolution, but just around the two emission peaks.
2. The 17 μm line follows a similar distribution to the 2.12 μm line and is clearly also shock-excited. In detail, it is somewhat more extended and relatively brighter towards Peak 2. We attribute this to the lower extinction for the line and a contribution from slower velocity ($\sim 5 \text{ km s}^{-1}$) shocks over a wider region of the source. The intrinsic H₂ line flux from Peak 2, accounting for its extra extinction, must be similar to that from Peak 1.
3. The 0-0 S(1)/1-0 S(1) line ratio is over an order of magnitude higher than expected in planar shock models, whether of C- or J-type.

4. The line flux is consistent, however, with an empirical planar J-shock cooling flow model where H_2 lines dominate the cooling.
5. It is also consistent with C-type bow-shock models in which we are observing the integrated emission from the entire bow. The magnetic fields required by such models, some tens of milligauss, are high.
6. By construction of a 'column density ratio' (*CDR*) curve from the available data it is clear that H_2 from a wide range of temperatures, a few hundred to several thousand Kelvin, is producing the emission observed in OMC-1. In particular, much of the gas contributing to the 0-0 S(1) line emission must be at temperatures very much less than 2000 K. Excitation temperatures defined between two levels of the H_2 molecule have limited applicability when determining the physical state of the source.
7. We predict the intensities of the pure rotational lines of H_2 at Peak 1, several of which have not yet been detected. In particular we anticipate the 28 μm 0-0 S(0) line having a flux of $\sim 2\%$ that of the 1-0 S(1) line through the same aperture.
8. We suggest that a consistent set of measurements of the lowest lying pure-rotational lines of H_2 , made with the same instrument, would provide stringent constraints on shock models.

Acknowledgements. A number of people have contributed to this study. We thank J. Baltz, S. Colgan, E. Erickson, S. Lord, A. Moorhouse and J. Simpson for their assistance with the observations. We acknowledge the efforts of the KAO staff and instrument support under UPN 352. The work benefitted greatly from conversations with Peter Brand and Michael Smith, who also kindly provided results from his model computations. MGB also wishes to thank the Institute for Astronomy in Edinburgh for their hospitality, during which much of this paper was written.

References

Allen D.A., Burton M.G. 1993, *Nat*, 363, 54
 Beckwith S., Evans N.J., Gatley I., Gull G., Russell R.W. 1983, *ApJ*, 264, 152
 Beckwith S., Persson S.E., Neugebauer G., Becklin E.E. 1978, *ApJ*, 223, 464
 Brand P.W.J.L. 1995a, *Ap&SS*, 224, 125
 Brand P.W.J.L. 1995b, *Ap&SS*, 233, 27
 Brand P.W.J.L., Moorhouse A., Burton M.G. et al. 1988, *ApJ*, 334, L103
 Burton M.G. 1992, *Aust. J. Phys.*, 45, 463
 Burton M.G., Puxley P. 1990, In: Hollenbach, D Thronson, H. (eds.), 2nd Wyoming Conf, The interstellar medium in external galaxies, NASA CP-3084, p238
 Burton M., Brand P., Moorhouse A., Geballe T. 1989, In: Kaldeich, B (ed) *Infrared Spectroscopy in Astronomy*, Proc. 22nd ESLAB symp. (ESA SP-290) p281
 Burton M.G., Hollenbach D.J., Tielens A.G.G.M. 1992, *ApJ*, 399, 563
 Chernoff D.F., Hollenbach D.J., McKee C.F. 1982, *ApJ*, 259, L97
 Chrysostomou A.C., Hough J.H., Burton M.G., Tamura M. 1994, *MNRAS*, 268, 325

Chrysostomou A.C., Burton M.G., Brand P.W.J.L. et al. 1997, *MNRAS*, submitted
 Dougados C., Lena P., Ridgeway S.T., Christou J.C., Probst R.G. 1993, *ApJ*, 406, 112
 Draine B.T. 1989, In: Kaldeich, B. (ed.) *Infrared Spectroscopy in Astronomy*, Proc 22nd ESLAB symp. (ESA SP-290), p93
 Draine B.T. 1991, In: Falgarone, E., Boulanger, F., Duvert, G. (eds.) *Proc. IAU Symp. 147, Fragmentation of Molecular Clouds and Star Formation*, p185
 Draine B.T., McKee C.F. 1993, *ARAA*, 31, 373
 Draine B.T., Roberge W.G., Dalgarno A. 1983, *ApJ*, 264, 485
 Erickson E.F., Haas M.R., Colgan S.W.J., Simpson J.P., Rubin R.H. 1995, In: Haas, M., Davidson, J. Erickson, E. (eds.) *ASP Conf. Series*, Vol. 73, *Airborne Astronomy Symposium on the Galactic Ecosystem: From Gas to Stars to Dust*, (San Francisco: ASP), p523
 Erickson E.F., Matthews S., Augason G.C. et al. 1984, *Proc. SPIE*, 509, 129
 Genzel R., Stutzki J. 1989, *ARAA*, 27, 41
 Haas M.R., Hollenbach D., Erickson E.F. 1991, *ApJ*, 374, 555
 Hollenbach D.J., Chernoff D.F., McKee C.F. 1989, In: Kaldeich, B. (ed.) *Infrared Spectroscopy in Astronomy*, Proc 22nd ESLAB symp. (ESA SP-290), p245
 Jennings D.E., Weber D.E., Brault J.W. 1987, *J. Mol. Spectr.*, 126, 19
 Kunze D., Rigopoulou D., Lutz D. et al. 1997, *A&A*, 315, 101
 Lord S. D. 1993, *NASA Technical Memorandum* 103957
 Moorwood A.F.M., Lutz D., Oliva E. et al. 1997, *A&A*, 315, 109
 Parmar P.S., Lacy J.H., Achtermann J.M. 1991, *ApJ*, 372, L25
 Parmar P.S., Lacy J.H., Achtermann J.M. 1994, *ApJ*, 430, 786
 Rigopoulou D., Lutz D., Genzel R. et al. 1997, *A&A*, 315, 125
 Simpson J.P., Cuzzi J.N., Erickson E.F., Strecker D.W., Tokunaga A.T. 1981, *Icarus*, 48, 230
 Smith M.D. 1991, *MNRAS*, 253, 175
 Smith M.D., Brand P.W.J.L. 1990, *MNRAS*, 245, 108
 Smith M.D., Brand P.W.J.L. Moorhouse A. 1991a, *MNRAS*, 248, 451
 Smith M.D., Brand P.W.J.L. Moorhouse A. 1991b, *MNRAS*, 248, 730
 Sturm E., Lutz D., Genzel R. et al. 1997, *A&A*, 315, 133
 Tedds J.A. 1996, *PhD Dissertation*, Univ. Edinburgh
 Timmermann R., Bertoldi F., Wright C.M. et al. 1997, *A&A*, 315, 281
 Wright C.M., Drapatz S., Timmermann R. et al. 1997, *A&A*, 315, 301